Jurnal Kejuruteraan 36(5) 2024: 2115–2120
https://doi.org/10.17576/jkukm-2024-36(5)-28

Effect of Scanning Speed on Microstructure Profile of Selective Laser Melted Stainless Steel 316L

Mohammad Azlan Aripin[a,d], Zainuddin Sajuri[a,b*], Nashrah Hani Jamadon[a,b], Intan Fadhlina Mohamed[a,b], Syarif Junaidi[c], Ahmad Muhammad Aziz[a] & Mohd Rhafiq Mazlan[a]

[a]*Department of Mechanical and Manufacturing Engineering, Faculty of Engineering and Built Enviroment, Universiti Kebangsaan Malaysia, 43600 Bangi, Selangor, Malaysia,*

[b]*Centre for Materials Engineering and Smart Manufacturing Faculty of Engineering and Built Environment, Universiti Kebangsaan Malaysia, 43600 Bangi, Selangor, Malaysia,*

[c]*Department of Mechanical and Nuclear Engineering, College of Engineering, University of Sharjah, 27272, United Arab Emirates,*

[d]*Department of Mechanical Engineering, Faculty of Engineering, City University 46100, Petaling Jaya, Malaysia*

**Corresponding author: zsajuri@ukm.edu.my*

Received 15 December 2023, Received in revised form 4 July 2024
Accepted 4 August 2024, Available online 30 September 2024

ABSTRACT

The selective laser melting (SLM) manufacturing process is currently gaining interest from various industries due to its ability to produce complex and hollow shapes. Processing parameters have been manipulated to obtain the best mechanical performance. However, the long production time remains the only major disadvantage compared to injection moulding. Production time can be decreased by increasing the scanning speed. This paper intends to investigate the effects of increasing scanning speed on the microstructural properties of SLM-produced stainless steel 316. Alteration of scanning speed directly affects the energy density and the thermal history of the parts. Two scanning speeds are used in the experiment with speed 750 mms^{-1} (V750) as the current default speed and 1400 mms^{-1} (V1400) for faster production time. The phases generated from each process were identified using the XRD test. The difference between austenite and ferrite in both samples is not distinct. High scanning speed results in slightly higher ferrite at 8.57% as compared to 6.03% for low scanning speed. It also yields lower austenite at 91.43% as compared to 93.97% at 750 mms^{-1}. The microstructure observation reveals V750 has deeper penetration and thinner melt pools. The higher energy density is related to the keyhole porosities found in the optical microscopy of V750 and thinner melt pools have enabled non-diffusion porosities at the side of melt pools. These findings will ultimately help the learning community to optimize the SLM processing parameters to achieve desired microstructural properties of 316L.

Keywords: Selective Laser Melting; Scanning Speed; Stainless Steel 316

INTRODUCTION

The advancement of SLM in the industry is hindered by its production speed. The production speed is rather slow to compete with faster manufacturing methods such as injection moulding. Scanning speed is a function of energy density, therefore ranges of scanning speed have been extensively studied by previous researchers to improve its tensile performance. For titanium alloy, increasing laser scan speed increases porosity due to the non-diffuse of powders and surface defects (Qiu et al. 2015). On the other hand, decreasing scanning speed leads to an excessive energy problem and introduces a splashing effect problem (Gong et al. 2014). These defects apply to stainless steel 316L. Previous study has successfully produced SLM-ed 316L below 1200 mms^{-1} (Collazo et al. 2022; Gao et al. 2020). According to Shanmuganathan et al. (2021),

decreasing scanning speed increases the area of melt pool boundary and overlapping hatch to reduce intertrack pores. The increment of scanning speed has an adverse effect such as increasing the porosity (Liu et al. 2020) and introducing a splashing effect that leads to microporosity (Wang et al. 2017). Few studies look into scanning speed above 1200 mms^{-1} and obtain optimum porosity (Bang et al. 2021; Khairallah et al. 2016; Vallejo et al. 2021). However, the microstructural profile in relation to respective scanning speeds is yet to be visualised and discussed in great depth.

The term austenitic stainless steel for 316 indicates that the material is primarily austenitic. There are a few methods used by previous researchers to identify and quantify the amount of phases that exist in microstructure namely EBSD (Salman et al. 2019) and XRD with the Rietveld method for phase volume fraction (Cegan et al. 2020; Saeidi et al. 2015). Phase identification studies obtained either a full austenitic phase (Zhang et al. 2021) or a small amount of ferrite (Marbury 2017). This is aligned with Schaeffler's diagram which estimates the amount of ferrite to be around 10% for 316 steel (Saboori et al. 2019). The martensitic phase is almost impossible to observe due to the low carbon content of 316 (Kamariah et al. 2020). The formation of microstructure especially the shape of ferrite can be predicted using the value of Cr-Ni equivalent in the 'Pseudo-binary predictive' phase diagram.

Apart from phase volume fraction, the melt pool geometry also plays an important role in comprehending the microstructural profile of SLM-ed 316L. The profile relies on the geometrical shape of the melt pool which can be measured from its width and depth (Ma et al. 2017). Both the depth and width of the molten pool vary with the laser and scanning speed. According to Wang et al., lower scanning speed results in higher peak temperatures that can induce the molten pool to be deeper. Correspondingly, the width or melt pool will be reduced. This may lead to certain types of porosity, such as lack-of-fusion porosity (Wang et al. 2020). Researchers have classified the types of defects respective to shapes either irregular or spherical (Collazo et al. 2022; Tucho et al. 2018) or contributing inducers such as power-induced or process-induced (Pham et al. 2020; Röttger et al. 2020; Tascioglu et al. 2020). Common types of defects arranged by increasing energy density, include gas porosity, surface balling, lack of fusion, layer void, spheroidisation and keyhole defect. Increasing the energy density at optimum levels will allow the observation of layer void along the melt pool boundary due to the thermal stress of adjacent melt pools (Liverani et al. 2017; Zhang et al. 2017). Excessive energy will yield keyhole defects and spheroidisation due to splashing effects (Cegan et al. 2020; Shi et al. 2020; Tucho et al. 2018). However, there is a lack of bridging of these porosities observation under a high scanning speed of more than 1200 mms^{-1}. Therefore this research intends to relate the microstructural profile including porosity for different scanning speeds through phase volume fraction analysis and visual observation from optical microscopy.

METHODOLOGY

MATERIAL AND PROCESSING PARAMETERS

This study begins by feeding layers of stainless steel 316L powders in the Renishaw Renam 500E SLM machine. The powders are laid down in a layer and impacted by a laser beam. As shown in Fig. 1(a), When the heat received from the laser is sufficient, the powders will melt in the form of a pool and hereby called a melt pool. The laser beam moved in a linear path with a scanning speed. Since this study focuses on the effect of scanning speed, there are two types of speed termed V750 with the speed of 750 mms^{-1} and V1400 for the sample with the speed of 1400 mms^{-1} as shown in Table 1. The difference speed yielded different values of energy density which were calculated using equation (1) which shows how the scanning speed contributes towards the energy density received by powder during the SLM process (Tucho et al. 2018).

$$E = \frac{P}{V\tau h} \tag{1}$$

Where E, energy input per volume, energy density (Jmm^{-2})

P, laser power (W)
V, scanning speed (mms^{-1})
τ, layer thickness (mm)
h, hatch spacing (mm)

TABLE 1. SLM process parameters.

Process Parameters	V750	V1400
Laser power	195 W	200 W
Laser scanning speed	750 mms^{-1}	1400 mms^{-1}
Layer thickness	50 µm	50 µm
Hatching distance	110 µm	110 µm
Temperature range	1371 – 1399 °C	1371 – 1399 °C
Heat treatment	Air-cooled	Air-cooled
Average powder size	55 µm	55 µm
Energy density	47.27 Jmm^{-3}	25.97 Jmm^{-3}

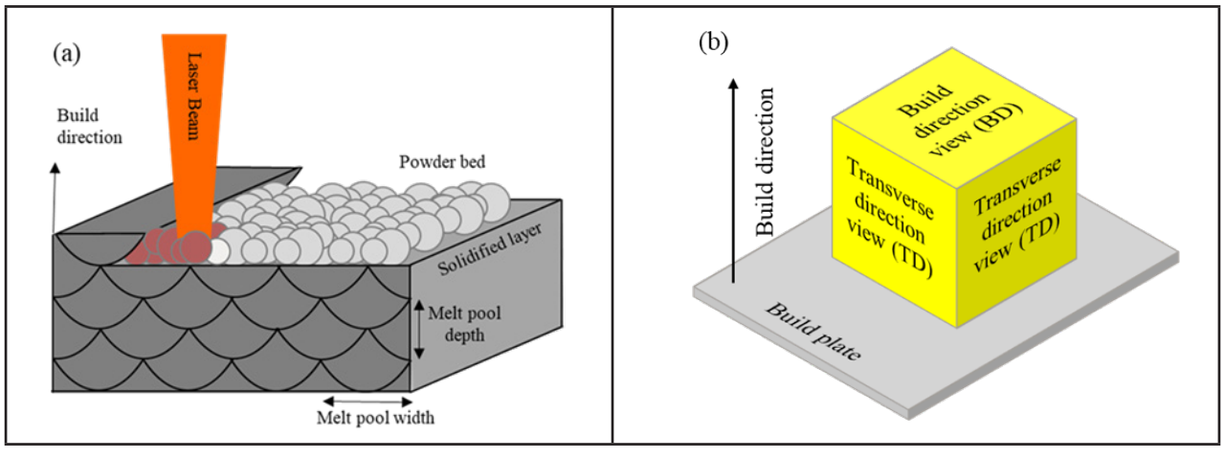

FIGURE 1. (a) Schematic diagram of the SLM process and (b) the respective view on a completed sample.

The completed solidified stainless steel 316L cube is then observed from the build direction and transverse view as shown in Fig. 1(b). To ensure a clear observation, the sample was mounted in Bakelite and ground using multiple grit papers starting from 400 to 1200 grit, followed by 1-micron diamond suspension polishing. The surface was immersed in Modified Fry's reagent for 10 s to reveal the final microstructure under optical microscopy. Apart from microscopy, XRD measurements were also made on the surface to identify the volume fraction of austenite and ferrite phases. This analysis was done using Bruker D8 Diffractometer that generated diffraction peaks in response to different compounds following the ASTM E975 standard (ASTM 2013).

RESULTS AND DISCUSSION

PHASE ANALYSIS

The XRD analysis in Fig. 2 indicates that sample V1400 has 91.43% austenite and 8.57% ferrite. There is no martensite observed as this phase is impossible to form due to low carbon content (Kamariah et al. 2020). Supposedly for 316L, 316L is fully austenite, due to non-equilibrium cooling, a small amount of delta ferrite is retained. Previous studies have shown the amount of ferrite is within the range of 5% to 10% maximum (Bedmar et al. 2021; Cegan et al. 2020; Marbury 2017). According to Zuback et al., this retained ferrite can be formed due to thermal cycles and microsegregation (Zuback & DebRoy 2018). In this study, the amount of ferrite is higher for sample V1400 at 8.57% compared to 6.03% in V750. The amount of austenite relies on the thermal history of the sample. A previous study has concluded that increasing the cooling rate will reduce the amount of ferrite (DebRoy et al. 2018). Since V750 experienced higher energy density, the cooling rate is higher in V750 which results in the lower ferrite.

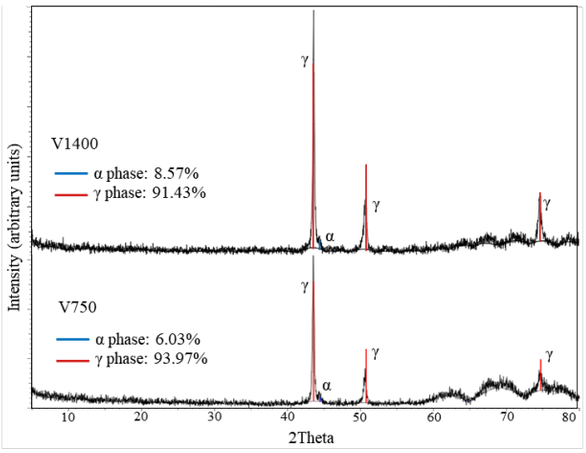

FIGURE 2. XRD analysis for phase volume fraction for samples V1400 and V750

MELT POOL PROFILE

In this study, there are two laser scanning speeds V750 and V1400 that result in energy density of 47.47 J/mm^2 and 25.97 J/mm^2. The higher energy density, V750 allow for deeper penetration of the melted pool. As shown in Fig. 3, the resulting melt pool was calculated by considering the average value of 7 layers of laser paths. For V750, the average depth is 49 µm slightly higher compared to 47 µm of V1400. The higher energy density provided by the laser in V750 has allowed for higher heat absorbed by metal powder and surrounding solidified layers. The surrounding layer may be remelted and diffused with the newly melted

powder. This allows for a new melt pool boundary at greater depth consistent with observations reported by past studies (Shanmuganathan et al. 2021; Waqar et al. 2021).

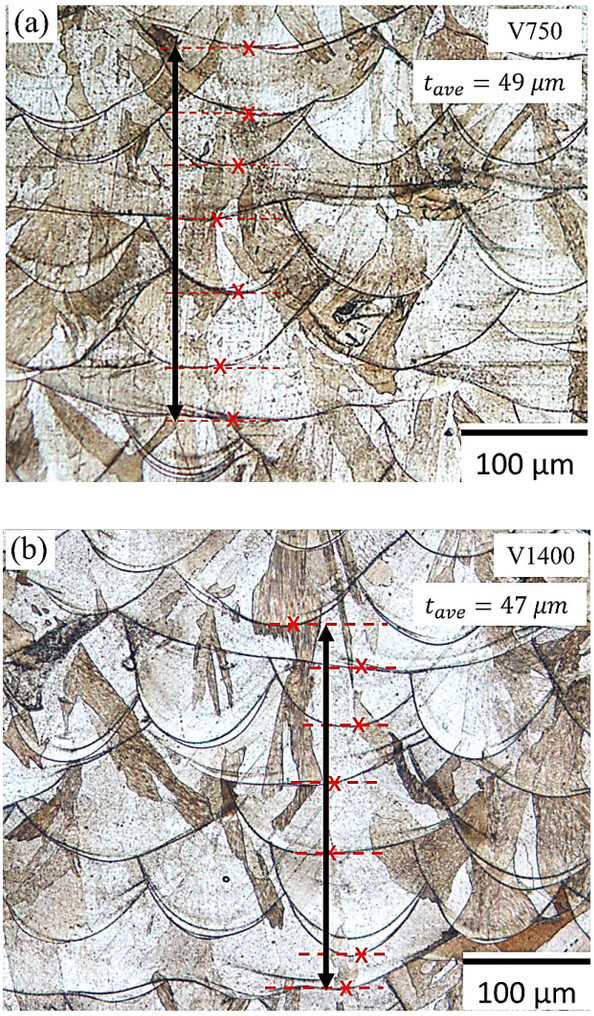

FIGURE 3. The resulting melt pool depth for scanning speed (a) V750 and (b) V1400

The distortion of melt pool geometry can be related to the types of porosity that can be observed. As shown in Fig. 4, the speed V750 has revealed two types of porosity namely keyhole and non diffuse porosity. These types of porosities are direct consequences of energy density supplied by the laser. Firstly, the keyhole porosity was greatly discussed by previous studies, where according to Tucho et al., if excessive energy density is supplied to powder, a violent reaction occurs which generates vaporization and spatter ejection. The vapour trapped in the voids remains in the middle of the melt pool. Secondly, the higher depth of the melt pool will lead to a distorted shape of the melt pool where it appears thinner than in ideal conditions. This compensated thinner geometry leads to non-diffuse at the side of the melt pool as shown in the Fig. 4(b). These two porosities will ultimately reduce the strength of the V750 material.

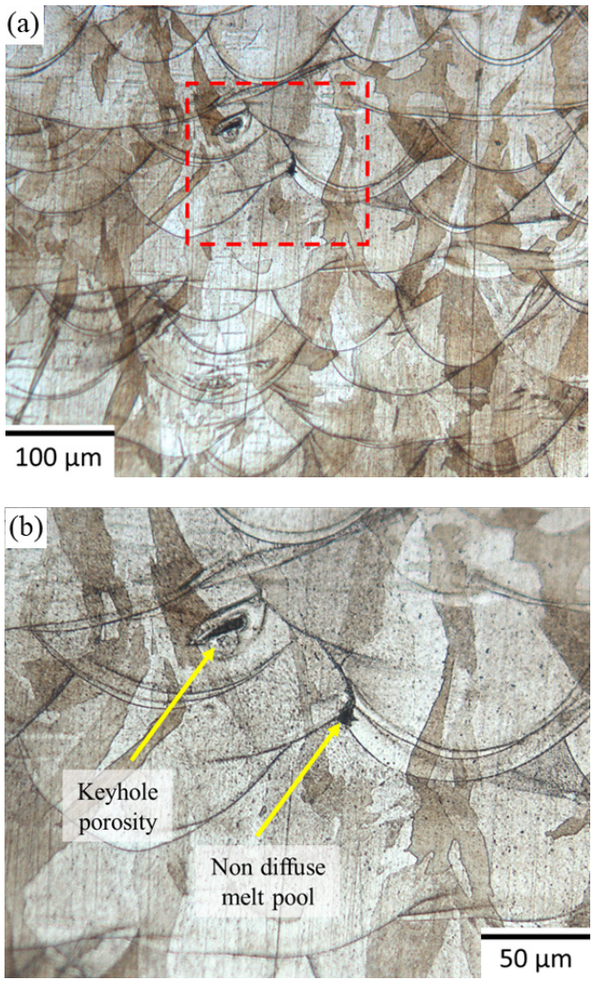

FIGURE 4. Keyhole porosity and non diffuse melt pool porosity observed for scanning speed V750 for (a) 10x zoom and (b) 20x zoom

CONCLUSION

This study was conducted to evaluate the melt pool geometry for different scanning speeds which were 750 mm/s and 1400 mm/s. Both scanning speed has an energy density of 47.27 J/mm3 and 25.97 J/mm3. The different energy densities result in different thermal histories where V750 has a higher cooling rate. This higher cooling rate results in lower ferrite content at 6.03% compared to 8.57% for V1400. Apart from that, higher energy density also influences the melt pool geometry where V750 has a deeper penetration and thinner melt pools. The higher energy density is related to the keyhole porosities found in the

optical microscopy of V750 and thinner melt pools have enabled non-diffusion porosities at the side of melt pools. These findings will ultimately help the learning community to optimize the SLM processing parameters to achieve desired microstructural properties that will potentially affect the mechanical properties. This will assist to improve the knowledge in the field of additive manufacturing and materials engineering, particularly in understanding the relationship between mechanical properties and geometrical properties of SLM 316.

ACKNOWLEDGEMENT

The authors would like to thank the Ministry of Higher Education Malaysia for supporting this research project through the Fundamental Research Grant Scheme FRGS/1/2019/TK03/UKM/02/3.

DECLARATION OF COMPETING INTEREST

None.

REFERENCES

American Society for Testing and Materials. 2013. *E975 Standard practice for X-ray determination of retained austenite in steel with near random crystallographic orientation*. ASTM. https://doi.org/10.1520/E0975-13

Bang, G. B., Kim, W. R., Kim, H. K., Park, H. K., Kim, G. H., Hyun, S. K., Kwon, O. & Kim, H. G. 2021. Effect of process parameters for selective laser melting with SUS316L on mechanical and microstructural properties with variation in chemical composition. *Materials Design* 197: 109221. https://doi.org/10.1016/j.matdes.2020.109221

Bedmar, J., Riquelme, A., Rodrigo, P., Torres, B. & Rams, J. 2021. Comparison of different additive manufacturing methods for 316L stainless steel. *Materials* 14. https://doi.org/10.3390/ma14216504

Cegan, T., Pagac, M., Jurica, J., Skotnicova, K., Hajnys, J., Horsak, L., Soucek, K. & Krpec, P. 2020. Effect of hot isostatic pressing on porosity and mechanical properties of 316L stainless steel prepared by the selective laser melting method. *Materials* 13: 1–26. https://doi.org/10.3390/ma13194377

Collazo, A., Figueroa, R., Pérez, C. & Nóvoa, X. R. 2022. Effect of laser speed and hatch spacing on the corrosion behavior of 316L stainless steel produced by selective laser melting. *Materials* 15: 1–18. https://doi.org/10.3390/ma15041353

DebRoy, T. Wei, H. L. Zuback, J. S. Mukherjee, T. Elmer, J. W. Milewski, J. O. Beese, A. M. Wilson-Heid, A. De, A. & Zhang, W. 2018. Additive manufacturing of metallic components – Process, structure and properties. *Progress in Materials Science* 92: 112–224. https://doi.org/10.1016/j.pmatsci.2017.10.001

Gao, S. Hu, Z. Duchamp, M. Krishnan, P. S. S. R. Tekumalla, S. Song, X. & Seita, M. 2020. Recrystallization-based grain boundary engineering of 316L stainless steel produced via selective laser melting. *Acta Materialia* 200: 366–377. https://doi.org/10.1016/j.actamat.2020.09.015

Gong, H. Gu, H. Zeng, K. Dilip, J. J. S. Pal, D. Stucker, B. Christiansen, D. Beuth, J. & Lewandowski, J. J. 2014. Melt pool characterization for selective laser melting of Ti-6Al-4V pre-alloyed powder. *25th Annual International Solid Freeform Fabrication Symposium: An Additive Manufacturing Conference* 256–267. https://doi.org/10.26153/tsw/15682

Kamariah, M. S. I. Harun, W. S. Ahmad, F. & Tarlochan, F. 2020. Mechanical behaviours of selective laser melting 316L stainless steel. *Journal of Additive Manufacturing & Advanced Materials* 1: 1–18. https://doi.org/10.1088/1757-899X/257/1/012021

Khairallah, S. A. Anderson, A. T. Rubenchik, A. & King, W. E. 2016. Laser powder-bed fusion additive manufacturing: Physics of complex melt flow and formation mechanisms of pores, spatter, and denudation zones. *Acta Materialia* 108: 36–45. https://doi.org/10.1016/j.actamat.2016.02.014

Liu, J. Song, Y. Chen, C. Wang, X. Li, H. Zhou, C. Wang, J. Guo, K. Sun, J. 2020. Effect of scanning speed on the microstructure and mechanical behavior of 316L stainless steel fabricated by selective laser melting. *Materials & Design* 186. https://doi.org/10.1016/j.matdes.2019.108355

Liverani, E. Toschi, S. Ceschini, L. & Fortunato, A. 2017. Effect of selective laser melting (SLM) process parameters on microstructure and mechanical properties of 316L austenitic stainless steel. *Journal of Materials Processing Technology* 249: 255–263. https://doi.org/10.1016/j.jmatprotec.2017.05.042

Ma, M. Wang, Z. & Zeng, X. 2017. A comparison on metallurgical behaviors of 316L stainless steel by selective laser melting and laser cladding deposition. *Materials Science and Engineering A* 685: 265–273. https://doi.org/10.1016/j.msea.2016.12.112

Marbury, F. 2017. Characterization of SLM printed 316L stainless steel and investigation of micro lattice geometry. *California Polytechnic State University*. https://doi.org/10.13140/RG.2.2.22470.29767

Pham, M. S. Dovgyy, B. Hooper, P. A. Gourlay, C. M. Piglione, A. 2020. The role of side-branching in microstructure development in laser powder-bed fusion. *Nature Communications* 11: 1–12. https://doi.org/10.1038/s41467-020-14453-3

Qiu, C. Panwisawas, C. Ward, M. Basoalto, H. C. Brooks, J. W. Attallah, M. M. 2015. On the role of melt flow into the surface structure and porosity development during selective laser melting. *Acta Materialia* 96: 72–79. https://doi.org/10.1016/j.actamat.2015.06.004

Röttger, A. Boes, J. Theisen, W. Thiele, M. Esen, C. Edelmann, A. & Hellmann, R. 2020. Microstructure and mechanical properties of 316L austenitic stainless steel processed by different SLM devices. *International Journal of Advanced Manufacturing Technology* 108: 769–783. https://doi.org/10.1007/s00170-020-05371-1

Saboori, A. Aversa, A. Bosio, F. Bassini, E. Librera, E. De Chirico, M. Biamino, S. Ugues, D. Fino, P. & Lombardi, M. 2019. An investigation on the effect of powder recycling on the microstructure and mechanical properties of AISI 316L produced by directed energy deposition. *Materials Science and Engineering: A* 766. https://doi.org/10.1016/j.msea.2019.138360

Saeidi, K. Gao, X. Lofaj, F. Kvetková, L. & Shen, Z. J. 2015. Transformation of austenite to duplex austenite-ferrite assembly in annealed stainless steel 316L consolidated by laser melting. *Journal of Alloys and Compounds* 633: 463–469. https://doi.org/10.1016/j.jallcom.2015.01.249

Salman, O. O. Gammer, C. Chaubey, A. K. Eckert, J. & Scudino, S. 2019. Effect of heat treatment on microstructure and mechanical properties of 316L steel synthesized by selective laser melting. *Materials Science and Engineering: A* 748: 205–212. https://doi.org/10.1016/j.msea.2019.01.110

Shanmuganathan, P. K. Purushothaman, D. B. & Ponnusamy, M. 2021. Effect of high laser energy density on selective laser melted 316L stainless steel: Analysis on metallurgical and mechanical properties and comparison with wrought 316L stainless steel. *3D Printing and Additive Manufacturing* https://doi.org/10.1089/3dp.2021.0061

Shi, W. Wang, P. Liu, Y. Hou, Y. & Han, G. 2020. Properties of 316L formed by a 400 W power laser selective laser melting with 250 μm layer thickness. *Powder Technology* 360: 151–164. https://doi.org/10.1016/j.powtec.2019.09.059

Tascioglu, E. Karabulut, Y. & Kaynak, Y. 2020. Correction to: Influence of heat treatment temperature on the microstructural, mechanical, and wear behavior of 316L stainless steel fabricated by laser powder bed additive manufacturing. *International Journal of Advanced Manufacturing Technology* 107: 1957. https://doi.org/10.1007/s00170-020-05115-1

Tucho, W. M. Lysne, V. H. Austbø, H. Sjolyst-Kverneland, A. & Hansen, V. 2018. Investigation of effects of process parameters on microstructure and hardness of SLM manufactured SS316L. *Journal of Alloys and Compounds* 740: 910–925. https://doi.org/10.1016/j.jallcom.2018.01.098

Vallejo, N. D. Lucas, C. Ayers, N. Graydon, K. Hyer, H. & Sohn, Y. 2021. Process optimization and microstructure analysis to understand laser powder bed fusion of 316L stainless steel. *Metals (Basel)* 11. https://doi.org/10.3390/met11050832

Wang, H. Wang, L. Cui, R. Wang, B. Luo, L. Su, Y. 2020. Differences in microstructure and nano-hardness of selective laser melted Inconel 718 single tracks under various melting modes of molten pool. *Journal of Materials Research and Technology* 9: 10401–10410. https://doi.org/10.1016/j.jmrt.2020.07.029

Wang, S. Liu, Y. Shi, W. Qi, B. Yang, J. Zhang, F. Han, D. & Ma, Y. 2017. Research on high layer thickness fabricated of 316L by selective laser melting. *Materials (Basel)* 10. https://doi.org/10.3390/ma10091055

Waqar, S. Sun, Q. Liu, J. Guo, K. & Sun, J. 2021. Numerical investigation of thermal behavior and melt pool morphology in multi-track multi-layer selective laser melting of the 316L steel. *International Journal of Advanced Manufacturing Technology* 112: 879–895. https://doi.org/10.1007/s00170-020-06360-0

Zhang, B. Li, Y. & Bai, Q. 2017. Defect formation mechanisms in selective laser melting: A review. *Chinese Journal of Mechanical Engineering (English Edition)* 30: 515–527. https://doi.org/10.1007/s10033-017-0121-5

Zhang, X. Kenesei, P. Park, J. S. Almer, J. & Li, M. 2021. In situ high-energy X-ray study of deformation mechanisms in additively manufactured 316L stainless steel. *Journal of Nuclear Materials* 549: 152874. https://doi.org/10.1016/j.jnucmat.2021.152874

Zuback, J. S. & DebRoy, T. 2018. The hardness of additively manufactured alloys. *Materials (Basel)*. https://doi.org/10.3390/ma11112070